

Electronic stopping power of protons and alpha particles in nickel

Edwin E. Quashie* and Alfredo A. Correa†

Quantum Simulations Group, Lawrence Livermore National Laboratory, Livermore, California 94550, USA

(Received 27 March 2018; revised manuscript received 22 October 2018; published 10 December 2018)

The electronic stopping power of nickel for protons and alpha particles at velocities below and around the Fermi velocity has been obtained to high accuracy using time-dependent density functional theory. For the wide range of projectile velocities considered, we observed different regimes of electronic stopping due to the alternative participation of *s*- and *d*-band electrons. Despite the sharp discontinuity in the electronic density of states near the Fermi energy characteristic of the nickel band structure, we do not find an anomalous nonlinear electronic stopping power limit as a function of velocity. However, we find a crossover region above $v = 0.15$ a.u. both for protons and alpha particles, related to the increase in participating host electrons and, in the case of alpha particles, to an increase of the charge state. We compare our calculated results with widely available experimental data and analyze the low velocity limits in the context of Lindhard's linear response theory and previous nonlinear density functional calculations. The comparison shows good accord with the lowest velocity experiments available. This may indicate that the adiabatic local density approximation is already a good theory to calculate electronic stopping power in materials at low velocity.

DOI: [10.1103/PhysRevB.98.235122](https://doi.org/10.1103/PhysRevB.98.235122)**I. INTRODUCTION**

Various theories have been developed to calculate electronic stopping power (S_e), ranging from the early perturbative methods of Bethe, Fermi-Teller, and Lindhard [1–4] to later nonperturbative methods on model systems [5–8]. However, it is only recently that numerical methods [9] have been able to directly tackle effects in the electronic stopping arising from the details of a realistic electronic structure of the host material at low projectile velocities, $v \ll v_{\text{Fermi}}$. With the advent of these new methods, Pruneda *et al.* [10] investigated threshold effects in wide-band gap insulators, Zeb *et al.* [11] studied the electronic stopping power in Gold (the role of *d* electrons and the H/He anomaly), Lim *et al.* [12] discovered the role of dynamical interstitial levels in semiconductors, and Quashie *et al.* [13] unveiled the effects of *d*-band electrons in copper. In these later cases, band structure effects, difficult to incorporate in early electronic stopping models are accounted for and shown to play a fundamental role [14].

Overall, the research mentioned above illustrates that the path towards low velocities of electronic stopping is not as simple (e.g., smooth and linear in v) as phenomenological models suggest [15]. The experimental evidence of deviations from linear velocity behavior and, for example, the role of *d* electrons was studied in Refs. [16–23]. Specifically for a copper host, a crossover region of superlinear velocity dependence (with a power of ~ 1.5) in the velocity range $v = 0.07$ – 0.3 a.u. (0.12 – 2.2 keV) of the electronic stopping of protons was shown to be associated with the copper electronic band structure, and in particular to the sharply peaked *d* band located at ~ 2 eV below the Fermi energy [13].

In terms of electronic band structure effects, a nickel host presents a more singular situation than copper, because the

Fermi level is precisely at the edge of the *d* band (see Fig. 5 in Ref. [24]). This gives rise to the intriguing possibility that the electronic stopping is superlinear even at extremely low velocities [25].

Additionally, nickel has shown important technological applications stemming from its resistance to particle radiation, as it was recently discovered that Ni-based random alloys can withstand swelling under particle radiation. Ni based alloys are known for their radiation tolerance, thermal stability, and optimal mechanical properties, making them promising candidate materials for nuclear applications [26].

In this paper, the case of S_e with emphasis on the low velocity limit of a nickel host under proton and alpha irradiation is presented. The comparison between proton and alpha irradiation helps us understand the nonlinear effects in the dielectric response and scaling laws with respect the projectile charge Z_1 .

The stopping power of protons and He_4^+ ions in nickel in the energy range of 20 to 95 keV was studied experimentally in detail by Bogdanov *et al.* [27]. Their measured results for energy losses of protons in nickel are in good agreement with those of Refs. [28,29] but in less agreement with Ref. [30]. These disagreements among experiments may stem from scaling issues related to measuring relative and absolute S_e . The measured energy losses of He_4^+ ions in nickel [27] are in good agreement with the measurements of Ref. [31].

Møller *et al.* [32] measured the stopping power of antiprotons (and protons) in various solid targets in the low-energy range of 1–100 keV. They found the stopping power of protons to be proportional to the projectile velocity below the stopping-power maximum for the Ni target, and simply compared the observation with a free electron gas model. Sillanpää *et al.* [33] determined, by indirect methods, the stopping power of He ions at velocities below the Bohr velocity in Mo; Cr; Cu and Ni targets; experimentally, the electronic stopping powers were deduced from the ion ranges

*quashie1@llnl.gov

†correaa@llnl.gov

using additional hypotheses about the nuclei interaction (ZBL potential [34]).

II. THEORETICAL AND COMPUTATIONAL DETAILS

In this work we employed the first-principles time-dependent Kohn-Sham formalism of time-dependent density functional theory (TDDFT) [35] coupled with nuclei motion [36,37] to simulate the collision dynamics of two different projectiles (hydrogen/proton and helium/alpha particles) in Ni target. The electron dynamics is treated quantum mechanically whereas the nuclei are point particles treated classically.

The exchange-correlation potential used in this study is due to the local-density approximation (LDA) of density functional theory (DFT) [38]. More sophisticated approaches based on the dielectric response, including the exact many-body and dynamic exchange-correlation treatment for low velocity projectiles, are available in the literature [39,40] and shown to be important for the stopping at least in the specific case of the *homogeneous* electron gas.

This *atomistic* calculation used a supercell with volume $(19.98a_0)^3$, containing 108 fcc host Ni atoms (experimental density) plus the projectile. Periodic boundary conditions along with Ewald-type summation [41–44] are used throughout this study. The plane-wave basis set is sampled accurately with a 160 Ry energy cutoff. For some selected velocities we tested k -point convergence in $(3 \times 3 \times 3)$ and $(4 \times 4 \times 4)$ Monkhorst-Pack grids [45], with a negligible difference of less than 0.1%. Finite size effects were studied for 108 and 256 atoms in supercells of $(3 \times 3 \times 3)$ and $(4 \times 4 \times 4)$ respectively, and the errors remain within 3% [13,46].

We used the norm-conserving Troullier-Martins pseudopotential to represent ion potentials V_{ext} , with 10 and 16 (to assess semicore effects) explicit electrons per Ni atom. The calculations were done using the QBOX/QBALL [47] with custom time-dependent modifications [9,48].

Initially, the projectiles (H or He) were placed in the Ni crystal interstitially to obtain a converged ground state by performing a *time-independent* DFT calculation. For the subsequent evolution of the moving projectile, a TDDFT calculation was then performed on the electronic system and the moving projectile. The projectile trajectory in the bulk crystal was done in two different ways: (i) hyperchanneling trajectory and (ii) off-channeling trajectory. In (i), the projectile is allowed to move with a given velocity subjected to a straight uniform movement along a $\langle 100 \rangle$ channel. This setup avoids collisions with target atoms [10,13,46,49,50]. In (ii), the projectile is forced to move in a *random* direction through the host material [13]. In this case, there is a stronger interaction between projectile and tightly bound electronic charge density in the vicinity of the host nuclei [13,46].

The wave functions are propagated in time using the fourth-order Runge-Kutta scheme [9] and the enforced time-reversal symmetry (ETRS) [51] method. The latter is more efficient for low projectile velocity calculations. We used these time integrators to ensure accurate propagation and forces at very low velocities. The propagation time step was set to, at most, 0.0242 attoseconds to ensure stable numerical integration [9,52].

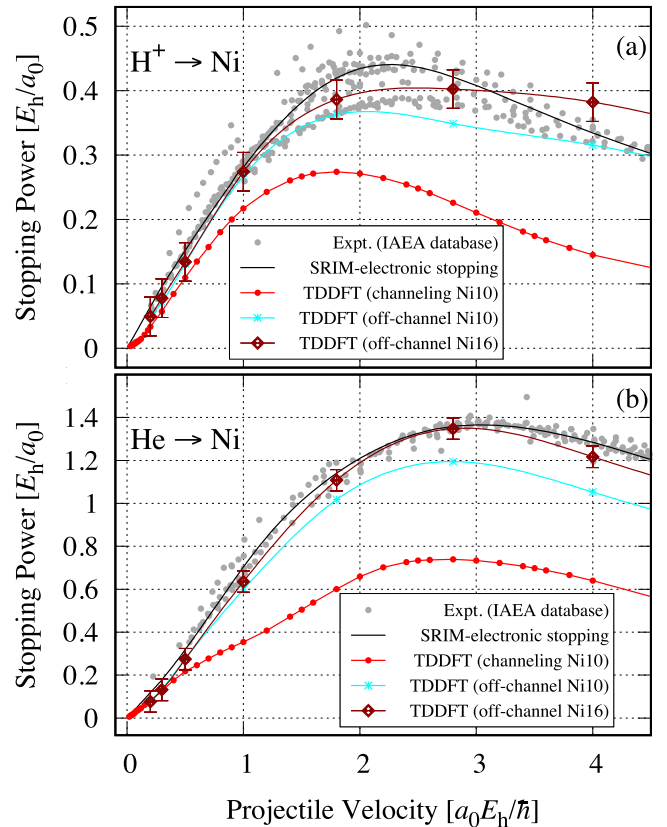


FIG. 1. H^+ and $He \rightarrow Ni$. The average S_e for (a) H^+ and (b) He versus projectile velocity v for channeling trajectory (red filled circles) without semicore, $[Ar]3d^84s^2$ (10 valence electrons) denoted as “TDDFT (channeling Ni10)”; off-channeling trajectory (cyan asterisks) without semicore, $[Ar]3d^84s^2$ (10 valence electrons) denoted as “TDDFT (off-channel Ni10)”; and off-channeling trajectory with semicore, $[Ne3s^2]3p^63d^84s^2$ (16 valence electrons) denoted as “TDDFT (off-channel Ni16).” The black continuous line refers to the empirically based tabulated electronic-stopping power model from SRIM [15,54]. The gray dots refer to the IAEA experimental database [55].

III. RESULTS AND DISCUSSION

As the simulated projectile position changes with time, energy is being deposited into the electronic subsystem. This increase in total electronic energy E as a function of projectile displacement is identified as the S_e given by the trajectory average [53]:

$$S_e = \left\langle \frac{dE[x(t)]}{dx(t)} \right\rangle \quad (1)$$

The calculated S_e for H^+ and He in Ni for a wide range of projectile velocities compared with empirical models and data are presented in Fig. 1. In the channeling case, where the projectile is forced to move in a straight path avoiding head-on collisions with the host atoms; the calculated S_e is systematically lower than that of experiments for both projectiles. We attribute this difference to the fact that the projectile lacks access to the full variety of trajectories that an experiment with uncontrolled directionality (e.g., with respect to a well defined crystal orientation) would provide.

We also performed simulations in off-channeling conditions where we allow the projectile to move in random directions, possibly closer to the host atoms. In most experimental setups, the projectiles are not channeled in any specific direction but rather are allowed to move in different directions and therefore explore different parts of the lattice. The use of random directions here are to specifically mimic the experimental setup, and was shown to work for other systems [13,46]. Doing so allows the projectile to seldom access core regions around the host atoms and thereby cause excitation of tightly bound electrons. Off-channeling trajectories are statistical in nature; averaging over different directions produces average values for stopping with a certain variance (shown as error bars in the graphs). The effective way to explore off-channeling trajectories is to move the projectile at several impact parameters (initial positions) and several velocity directions, and average over these different projectile initial positions and velocity directions. Here we used two main velocity incommensurate directions, [0.309, 0.5, 0.809] and [0.705, 0.610, 0.363], with their corresponding permutations making a total of 12 velocity directions to obtain our off-channeling results.

In the off-channeling trajectories case, we studied two levels of pseudopotentials. First, we simulated the electronic system with a pseudopotential not including semi-core electrons in the valence (10 electrons per host atom, $3d^84s^2$), while the rest of electrons, in particular the $3p^6$, are frozen and taken into account only as part of the pseudopotential. Second, to assess the role of semicore electrons we used a different pseudopotential including some semicore electrons in valence; we simulated 16 electrons ($3p^63d^84s^2$) per host atom. In the calculation, the charge of the projectile is not chosen *a priori*; in the steady state the average charge state of the projectile is determined by the time evolution of the system.

For H^+ in Fig. 1(a), we obtained fairly good agreement with experiment in a wide range of velocities, as long as we consider off-channeling and include host semicore electrons explicitly. Semicore electron effects kick in at $v > 1.5$ a.u. and the correction is similar ($\sim 10\%$) in both cases (H^+ and He). The difference between off-channeling and channeling is appreciable for $v > 1.0$ a.u., and is particularly important in the case of alpha projectiles; although, it is seen that at velocities above 3.0 a.u. our off-channeling results go over the experimental data. On the other hand, the agreement with experiment is excellent for $v \leq 3.0$ a.u. for He in Fig. 1(b). At $v > 3.0$ a.u., our results underestimate experiment, indicating even more semicore electrons would need to be incorporated in the Ni pseudopotential if we were to explore higher velocities [56]. At lower velocities, both channeling and off-channeling trajectories collapse into one curve; this apparent independence on the geometry of the trajectory follows a pattern observed in previous simulations [13,50,57].

In Fig. 2 and 3 we concentrate on the low velocity limit and compare with the available experimental data and theory. In Fig. 2, for the range $0.2 < v < 5$ a.u. our calculated S_e for off-channeling protons is compared with experiments [15,27,32,58,59]. As an example, for $v \sim 0.2$ a.u. our channeling result is $\sim 10\%$ below compared with that of Andersen *et al.* [59]. There are few experimental data for $v < 0.2$ a.u.

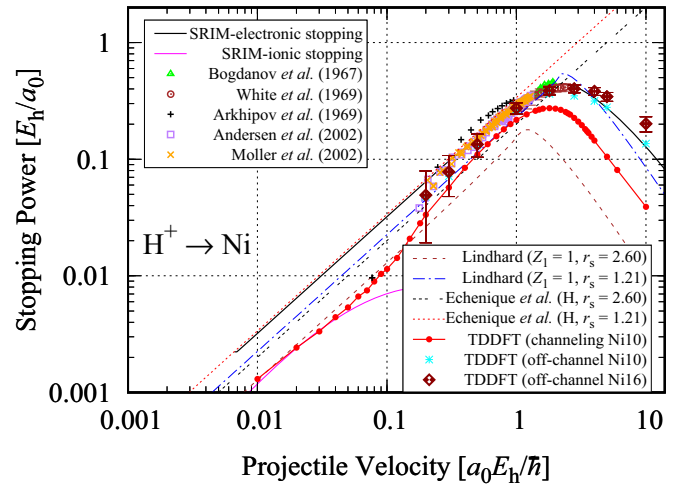


FIG. 2. $H^+ \rightarrow Ni$ (log scale). The average S_e versus projectile velocity v for a channeling trajectory (red circles) without semicore, $[Ar]3d^84s^2$ (10 valence electrons) denoted as “TDDFT (channeling Ni10)”; off-channeling trajectory (cyan asterisks) without semicore, $[Ar]3d^84s^2$ (10 valence electrons) denoted as “TDDFT (off-channel Ni10)”; and off-channeling trajectory with semicore, $[Ne3s^2]3p^63d^84s^2$ (16 valence electrons) denoted as “TDDFT (off-channel Ni16).” The dashed (brown) line and dash-dotted (blue) line correspond to linear RPA-based calculations for a free-electron gas with $r_s = 2.60a_0$ and $r_s = 1.21a_0$, where the effective charge of the H^+ projectile is $Z_1 = 1$ [Eq. (2)]. The triple-dashed (black) line and dotted (red) line correspond to DFT results (slopes) for protons by Echenique *et al.* [7] (see Fig. 3, curve “D”) with $r_s = 2.60a_0$ and $r_s = 1.21a_0$ (which nominally correspond to 1 and 10 electrons per Ni atom respectively). The tabulated results from the SRIM empirical model for the electronic and ionic stopping powers of protons are represented by the solid black and solid magenta lines, respectively [15].

However, at $v \sim 0.08$ a.u., our TDDFT (channeling Ni10) result for protons is in good agreement with that of Arkhipov *et al.* [60], with 5% difference.

In Fig. 3, our results show that the relatively heavier He projectile result agrees well with that of Sillanpää *et al.* [33] (an indirect experimental result) in their velocity range ($0.01 \leq v \leq 0.1$ a.u.). More experimental work in this velocity regime would be required to validate the capability of our *ab initio* TDDFT method. The lack of experimental data at $v < 0.01$ a.u. makes it difficult to validate our predictive result below this velocity regime. For higher velocity, our calculated results are in agreement with experimental data [27,33,58,61–63].

To analyze the behavior of the simulated S_e in detail, we evaluated the linear response stopping based on the Lindhard dielectric function for a homogeneous electron gas for effective electronic densities n [4,64–67]:

$$S_L(n, v) = \frac{2Z_1^2 e^2}{\pi v^2} \int_0^\infty \frac{dk}{k} \int_0^{kv} \omega d\omega \text{Im}(\epsilon_{RPA}[n, k, \omega]^{-1}), \quad (2)$$

where Z_1 is the charge of the projectile (ion) (for example, $Z_1 = 1$ for H^+ and $Z_1 = 2$ for a *fully stripped* He^{2+} ion), v is the velocity of the projectile, and ϵ_{RPA} is a model of

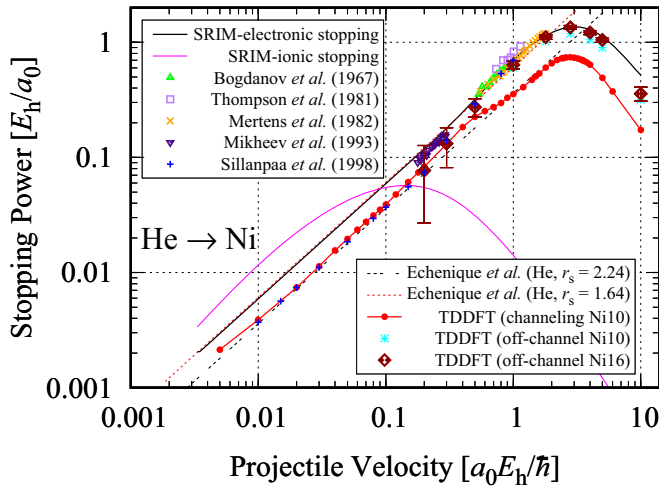


FIG. 3. He \rightarrow Ni (log scale). The average S_e versus projectile velocity v for a channeling trajectory (red circles) without semicore, [Ar]3d⁸4s² (10 valence electrons) denoted as “TDDFT (channeling Ni10)”; off-channeling trajectory (cyan asterisks) without semicore, [Ar]3d⁸4s² (10 valence electrons) denoted as “TDDFT (off-channel Ni10)”; and off-channeling trajectory with semicore, [Ne3s²]3p⁶3d⁸4s² (16 valence electrons) denoted as “TDDFT (off-channel Ni16).” The triple-dashed (black) line and dotted (red) line correspond to DFT results (slopes) for a helium nucleus by Echenique *et al.* [7] with adjusted $r_s = 2.24a_0$ and $r_s = 1.64a_0$ (which nominally correspond to 1.57 and 4 electrons per Ni atom respectively). The tabulated results from the SRIM database for the electronic and ionic stopping powers are represented by the solid black and solid magenta lines, respectively [15].

the dielectric function for the linear response approximation (RPA) at frequency ω and momentum transfer k for an electron gas with effective density n [68]. The linear-response approximation to the stopping power is relatively crude compared to the TDDFT simulation results presented here, but we compare the two here to understand with a simpler model our full TDDFT calculations in different limits. In order to compare to a more elaborate model, we compare it with nonlinear DFT calculations of stopping power which are formally exact for the homogeneous electron gas in the limit of $v \rightarrow 0$ reported in [7] for both H and He and parametrized by density n . For reference, we used $n = 9.1 \times 10^{22}/\text{cm}^3$, $n = 36.6 \times 10^{22}/\text{cm}^3$, $n = 91.4 \times 10^{22}/\text{cm}^3$, and $n = 146.2 \times 10^{22}/\text{cm}^3$, corresponding nominally to 1e ($r_s = 2.60a_0$), 4e ($r_s = 1.64a_0$), 10e ($r_s = 1.21a_0$), and 16e ($r_s = 1.03a_0$) per Ni atom respectively.

In Fig. 2 our simulated TDDFT results at low velocities for proton projectiles correspond well with linear response stopping (S_L) where $r_s = 2.60a_0$ ($Z_1 = 1$). Our TDDFT results agree well with DFT results of Echenique *et al.* (see Fig. 3, curve “D” of Ref. [7]) for $r_s = 1.21a_0$ around $0.2 \leq v \leq 1.0$ a.u., but at lower velocities ($v < 0.1$ a.u.) their DFT results for $r_s = 2.60a_0$ overestimate our TDDFT results. Although there are two independent parameters to adjust in the Lindhard model (Z_1 and n), a picture in which $Z_1 \equiv 1$ (independent of velocity) seems reasonable for protons, since hydrogen loses its electron easily in a metallic environment [69].

We observe that, for protons, S_e falls to values near the nuclear stopping estimated by the most current version of SRIM. Also, according to our results, the SRIM extrapolation ($v \rightarrow 0$) model is systematically overestimating the electronic stopping by a factor 2 or 3 for both types of projectiles. We again observe a crossover region for protons (as seen in the Cu result [13]). For $0.15 \leq v \leq 0.5$ a.u. crossover region, the curve is a power law $\propto v^q$ where $q = 1.32$. We do not find nonlinearities as a function of velocity below 0.15 a.u., in agreement with the expected analytic result for normal metallic stopping power.

For He, the linear response approximation is out of range at low velocity because of the dominance of nonlinear effects and variable effective charges. For this reason, in Fig. 3 we only rely on the nonlinear DFT ($v \rightarrow 0$) slopes reported by Echenique *et al.* (see Fig. 3, curve “E” in Ref. [7]), which agree well with our TDDFT result when an adjusted $r_s = 2.24a_0$ is used, which in turn corresponds to $Z_1^* = 1.2$ (according to Fig. 4 in Ref. [7]). At higher velocity the comparison is not as straightforward, but a preliminary adjustment to Ref. [7] gives an effective $r_s = 1.64a_0$ and $Z_1^* = 1.5$, respectively, for $0.5 < v < 2.0$ a.u. (off-channeling). That is, more charge is being stripped off from the He projectile and more valence electrons participate [70].

IV. CONCLUSIONS

In summary, we obtained accurate results for the electronic stopping power of protons and alpha particles in Nickel. Despite the d band being very close to the Fermi energy, the electronic stopping does not follow an anomalous electronic stopping power in the limit $v \rightarrow 0$. The electronic stopping power is linear with the velocity, similar to the linear response of the homogeneous electron gas. As in the case of Cu [13], we observe a crossover region of superlinear stopping power for the proton in Ni, but only for $v > 0.15$ a.u.

In the case of the alpha particle, the stopping power is more linear with respect to velocity. There is no crossover region for alpha particles, and the only feature appears at $v > 0.5$ a.u., due to the consideration of off-channeling trajectories.

The resulting stopping power is in surprisingly good agreement with the experimental determinations at extremely low velocities for both protons and alpha particles [33,60], even when utilizing the simple adiabatic local density approximation (ALDA) to the electronic exchange correlation. Although nonlocal theories based on many-body physics for dynamic exchange correlation were previously shown to be necessary in the case of the homogeneous electron gas in the limit of low velocity [39,40], we achieved the *ab initio* calculation of electronic stopping power at the lowest velocity to date and we do not seem to find further corrections to exchange correlation to be a key element to account for in the calculation of electronic stopping for these projectiles and realistic materials.

Note added in proof. Recently, we became aware of new experimental work by Roth *et al.* [71].

ACKNOWLEDGMENTS

We thank J. M. Pitarke for constructive discussions of the nonlocal exchange-correlation in time-dependent current

density functional theory. This work was performed under the auspices of the U.S. Department of Energy by Lawrence Livermore National Laboratory under Contract No. DE-AC52-07NA27344. This work was supported as part of Energy Dissipation to Defect Evolution (EDDE), an Energy Fron-

tier Research Center funded by the U.S. Department of Energy, Office of Science under Contract No. DE-AC05-00OR22725. Computing support for this work came from the Lawrence Livermore National Laboratory Institutional Computing Grand Challenge program.

-
- [1] H. Bethe, *Ann. Phys. (N.Y.)* **397**, 325 (1930).
[2] F. Bloch, *Ann. Phys. (N.Y.)* **408**, 285 (1933).
[3] E. Fermi and E. Teller, *Phys. Rev.* **72**, 399 (1947).
[4] J. Lindhard, *Phys. Lett.* **12**, 126 (1964).
[5] P. Echenique, R. Nieminen, and R. Ritchie, *Solid State Commun.* **37**, 779 (1981).
[6] M. J. Puska and R. M. Nieminen, *Phys. Rev. B* **27**, 6121 (1983).
[7] P. M. Echenique, R. M. Nieminen, J. C. Ashley, and R. H. Ritchie, *Phys. Rev. A* **33**, 897 (1986).
[8] P. M. Echenique, I. Nagy, and A. Arnau, *Int. J. Quantum Chem.* **36**, 521 (2009).
[9] A. Schleife, E. W. Draeger, Y. Kanai, and A. A. Correa, *J. Chem. Phys.* **137**, 22A546 (2012).
[10] J. M. Pruneda, D. Sánchez-Portal, A. Arnau, J. I. Juaristi, and E. Artacho, *Phys. Rev. Lett.* **99**, 235501 (2007).
[11] M. A. Zeb, J. Kohanoff, D. Sánchez-Portal, A. Arnau, J. I. Juaristi, and E. Artacho, *Phys. Rev. Lett.* **108**, 225504 (2012).
[12] A. Lim, W. M. C. Foulkes, A. P. Horsfield, D. R. Mason, A. Schleife, E. W. Draeger, and A. A. Correa, *Phys. Rev. Lett.* **116**, 043201 (2016).
[13] E. E. Quashie, B. C. Saha, and A. A. Correa, *Phys. Rev. B* **94**, 155403 (2016).
[14] E. Artacho, *J. Phys.: Condens. Matter* **19**, 275211 (2007).
[15] J. F. Ziegler, M. Ziegler, and J. Biersack, *Nucl. Instrum. Methods Phys. Res., Sect. B* **268**, 1818 (2010).
[16] R. Blume, W. Eckstein, and H. Verbeek, in *Ion Beam Analysis*, edited by H. H. Andersen, J. Böttiger, and H. Knudsen (Elsevier, North Holland, 1980), pp. 57–62.
[17] J. E. Valdés, J. C. Eckardt, G. H. Lantschner, and N. R. Arista, *Phys. Rev. A* **49**, 1083 (1994).
[18] E. A. Figueroa, E. D. Cantero, J. C. Eckardt, G. H. Lantschner, J. E. Valdés, and N. R. Arista, *Phys. Rev. A* **75**, 010901(R) (2007).
[19] S. N. Markin, D. Primetzhofer, S. Prusa, M. Brunmayr, G. Kowarik, F. Aumayr, and P. Bauer, *Phys. Rev. B* **78**, 195122 (2008).
[20] E. D. Cantero, R. C. Fadanelli, C. C. Montanari, M. Behar, J. C. Eckardt, G. H. Lantschner, J. E. Miraglia, and N. R. Arista, *Phys. Rev. A* **79**, 042904 (2009).
[21] D. Goebel, D. Roth, and P. Bauer, *Phys. Rev. A* **87**, 062903 (2013).
[22] D. Roth, B. Bruckner, M. Moro, S. Gruber, D. Goebel, J. Juaristi, M. Alducin, R. Steinberger, J. Duchoslav, D. Primetzhofer, and P. Bauer, *Phys. Rev. Lett.* **118**, 103401 (2017).
[23] D. Roth, B. Bruckner, G. Undeutsch, V. Paneta, A. Mardare, C. McGahan, M. Dosmailov, J. Juaristi, M. Alducin, J. Pedarnig, R. Haglund, D. Primetzhofer, and P. Bauer, *Phys. Rev. Lett.* **119**, 163401 (2017).
[24] Z. Lin, L. V. Zhigilei, and V. Celli, *Phys. Rev. B* **77**, 075133 (2008).
[25] J. M. Fernández-Varea and N. R. Arista, *Radiat. Phys. Chem.* **96**, 88 (2014).
[26] Y. Zhang, K. Jin, H. Xue, C. Lu, R. J. Olsen, L. K. Beland, M. W. Ullah, S. Zhao, H. Bei, D. S. Aidhy, G. D. Samolyuk, L. Wang, M. Caro, A. Caro, G. M. Stocks, B. C. Larson, I. M. Robertson, A. A. Correa, and W. J. Weber, *J. Mater. Res.* **31**, 2363 (2016).
[27] G. F. Bogdanov, V. P. Kabaev, F. V. Lebedev, and G. M. Novikov, *Sov. At. Energy* **22**, 133 (1967).
[28] A. B. Chilton, J. N. Cooper, and J. C. Harris, *Phys. Rev.* **93**, 413 (1954).
[29] M. Bader, R. E. Pixley, F. S. Mozer, and W. Whaling, *Phys. Rev.* **103**, 32 (1956).
[30] G. M. Osetinskii, *At. Energ. [Sov. J. At. Energy]* **94**, 5 (1957), Suppl. 5, in Russian.
[31] S. K. Allison, *Rev. Mod. Phys.* **30**, 1137 (1958).
[32] S. P. Møller, A. Csete, T. Ichioka, H. Knudsen, U. I. Uggerhøj, and H. H. Andersen, *Phys. Rev. Lett.* **88**, 193201 (2002).
[33] J. Sillanpää, E. Vainonen-Ahlgren, P. Haussalo, and J. Keinonen, *Nucl. Instrum. Methods Phys. Res., Sect. B* **142**, 1 (1998).
[34] J. F. Ziegler, U. Littmark, and J. P. Biersack, *The Stopping and Range of Ions in Solids* (Pergamon, New York, 1985), Vol. 1.
[35] C. A. Ullrich, *Time-Dependent Density-Functional Theory* (Oxford University Press, Oxford, 2011).
[36] E. K. U. Gross, J. F. Dobson, and M. Petersilka, in *Density Functional Theory II: Relativistic and Time Dependent Extensions*, edited by R. F. Nalewajski, Topics in Current Chemistry (Springer-Verlag, Berlin, 1996), Vol. 181, pp. 81–172.
[37] X. Andrade, A. Castro, D. Zueco, J. L. Alonso, P. Echenique, F. Falceto, and Á. Rubio, *J. Chem. Theory Comput.* **5**, 728 (2009).
[38] J. P. Perdew and A. Zunger, *Phys. Rev. B* **23**, 5048 (1981).
[39] V. U. Nazarov, J. M. Pitarke, C. S. Kim, and Y. Takada, *Phys. Rev. B* **71**, 121106 (2005).
[40] V. U. Nazarov, J. M. Pitarke, Y. Takada, G. Vignale, and Y.-C. Chang, *Phys. Rev. B* **76**, 205103 (2007).
[41] J. Kolafa and J. W. Perram, *Mol. Simul.* **9**, 351 (1992).
[42] H. D. Hecce, A. E. Garcia, and T. Darden, *J. Chem. Phys.* **126**, 124106 (2007).
[43] B. A. Wells and A. L. Chaffee, *J. Chem. Theory Comput.* **11**, 3684 (2015).
[44] A. Bródka, *Chem. Phys. Lett.* **400**, 62 (2004).
[45] H. J. Monkhorst and J. D. Pack, *Phys. Rev. B* **13**, 5188 (1976).
[46] A. Schleife, Y. Kanai, and A. A. Correa, *Phys. Rev. B* **91**, 014306 (2015).
[47] F. Gygi, *IBM J. Res. Dev.* **52**, 137 (2008).
[48] E. W. Draeger, X. Andrade, J. A. Gunnels, A. Bhatlele, A. Schleife, and A. A. Correa, in *2016 IEEE International Parallel and Distributed Processing Symposium (IPDPS)*, Chicago, May 2016 (IEEE, Piscataway, NJ, 2016), pp. 832–841.
[49] J. M. Pruneda and E. Artacho, *Phys. Rev. B* **71**, 094113 (2005).

- [50] A. A. Correa, J. Kohanoff, E. Artacho, D. Sánchez-Portal, and A. Caro, *Phys. Rev. Lett.* **108**, 213201 (2012).
- [51] A. Castro, M. A. L. Marques, and A. Rubio, *J. Chem. Phys.* **121**, 3425 (2004).
- [52] A. Gómez Pueyo, M. A. L. Marques, A. Rubio, and A. Castro, *J. Chem. Theory Comput.* **14**, 3040 (2018).
- [53] A. A. Correa, *Comput. Mater. Sci.* **150**, 291 (2018).
- [54] J. F. Ziegler, <http://www.srim.org/SRIM/SRIMPICS/STOP01/STOP0128.gif>.
- [55] Stopping Power of Matter for Ions: Graphs, Data, Comments and Programs (last updated Dec 18, 2017), http://www-nds.iaea.org/stopping/stopping_hydr.html.
- [56] R. Ullah, E. Artacho, and A. A. Correa, *Phys. Rev. Lett.* **121**, 116401 (2018).
- [57] R. Ullah, F. Corsetti, D. Sánchez-Portal, and E. Artacho, *Phys. Rev. B* **91**, 125203 (2015).
- [58] W. White and R. M. Mueller, *Phys. Rev.* **187**, 499 (1969).
- [59] H. Andersen, A. Csete, T. Ichioka, H. Knudsen, S. Møller, and U. Uggerhøj, *Nucl. Instrum. Methods Phys. Res., Sect. B* **194**, 217 (2002).
- [60] E. P. Arkhipov and Y. V. Gott, *Sov. Phys. JETP* **29**, 615 (1969).
- [61] D. Thompson, W. Poehlman, P. Presunka, and J. Davies, *Nucl. Instrum. Methods Phys. Res.* **191**, 469 (1981).
- [62] P. Mertens and T. Krist, *J. Appl. Phys.* **53**, 7343 (1982).
- [63] S. Mikheev, Y. Ryzhov, I. Shkarban, and V. Yurasova, *Nucl. Instrum. Methods Phys. Res., Sect. B* **78**, 86 (1993).
- [64] J. Lindhard and M. Scharff, *K. Dan. Vidensk. Selsk. Mat. Fys. Medd.* **27**, 15 (1953).
- [65] J. Lindhard and A. Winther, *K. Dan. Vidensk. Selsk. Mat. Fys. Medd.* **34**, 1 (1964).
- [66] J. Lindhard, *K. Dan. Vidensk. Selsk. Mat. Fys. Medd.* **28**, 1 (1954).
- [67] J. Lindhard and A. Winther, *Stopping Power of Electron Gas and Equipartition Rule*, Kongelige Danske videnskabernes selskab Matematisk-fysiske meddelelser (Munksgaard, Copenhagen, 1964).
- [68] G. Giuliani and G. Vignale, *Quantum Theory of the Electron Liquid* (Cambridge University Press, Cambridge, 2008).
- [69] N. Arista, *Mat. Fys. Medd. K. Dan. Vidensk. Selsk.* **52**, 595 (2006).
- [70] A. Arnau, M. Peñalba, P. Echenique, and F. Flores, *Nucl. Instrum. Methods Phys. Res., Sect. B* **69**, 102 (1992).
- [71] D. Roth, C. E. Celedon, D. Goebel, E. A. Sanchez, B. Bruckner, R. Steinberger, J. Guimpel, N. R. Arista, and P. Bauer, *Nucl. Instrum. Methods Phys. Res., Sect. B* **437**, 1 (2018).